Adsorption on transition metal surfaces: Transferability and accuracy of DFT using the ADS41 dataset

Shaama Mallikarjun Sharada,[1] Rasmus K. B. Karlsson,[2,3,*] Yasheng Maimaiti,[2,3] Johannes Voss,[2,3] and Thomas Bligaard[2,3]

[1]*Mork Family Department of Chemical Engineering and Materials Science, University of Southern California, 925 Bloom Walk, Los Angeles, California 90089, USA*

[2]*Department of Chemical Engineering, Stanford University, 443 Via Ortega, Stanford California 94305, USA*

[3]*SUNCAT Center for Interface Science and Catalysis, SLAC National Accelerator Laboratory, Menlo Park, California 94025, USA*

We present a benchmarking study of adsorption energies on transition metal surfaces computed with select functionals across different density functional theory codes. In addition to gradient corrected functionals, we evaluate the accuracies of representative metaGGAs, including MS2, SCAN, and SCAN+rVV10, as well as a short-range screened hybrid functional, HSE06. The study shows that the challenge of finding a functional that can simultaneously capture both covalent and noncovalent molecule-surface interactions persists, with no single functional in the benchmarking study with average errors <0.2 eV. We find that HSE06 on average does not improve the accuracy compared to PBE for the surface chemistry of transition metals. The BEEF-vdW dispersion-corrected generalized gradient approximation (GGA) and the MS2 metaGGA yield the lowest errors in both chemisorption and dispersion energies, demonstrating that moving up the Jacob's ladder of functionals to screened hybrids does not necessarily improve the description of transition metal surface chemistry.

DOI: 10.1103/PhysRevB.100.035439

I. INTRODUCTION

The description of molecule-surface interactions poses a significant challenge for Kohn-Sham density functional theory (KS-DFT) [1,2]. This is because the most widely used functionals, generalized gradient approximations (GGAs), can accurately describe either bulk systems or gas phase thermochemistry but rarely both [3]. One of the reasons contributing to this difficulty is the dearth of highly accurate surface chemistry datasets that are necessary to benchmark [4] and train density functionals. Various commonly used density functionals have been benchmarked by comparing calculated values of atomic structure data, cohesive energies, and bulk moduli of all transition metals to available experimental data [5,6]. A recent study by Vega *et al.* that benchmarks bulk and surface properties for fcc metals using various GGAs and metaGGAs showed that no functional can accurately describe all surface properties [7]. Datasets for properties of gas phase molecules can be created using the highly expensive but accurate quantum methods such as the quantum chemistry "gold standard" CCSD(T) [8]. Since these methods are prohibitive for periodic systems, research in this field has been focused on the careful collation of highly accurate, single-crystal experimental data to benchmark theoretical predictions.

The CE39 dataset, developed recently in this group, is a compilation of experimental adsorption energies on ten different transition metal surfaces [9]. The CE39 study also contrasts the performance of local density approximations (LDA), several GGAs, and the BEEF-vdW dispersion-corrected GGA, and concludes that while RPBE and BEEF-vdW can accurately predict chemisorption energies, there is room for improving the description of dispersion-bound systems [9]. Later studies employed the CE39 dataset to benchmark the performance of Minnesota metaGGAs [10] and to develop an interpolation approximation between a GGA and a GGA-vdW [11] for improved estimates of adsorption energies. A larger dataset, consisting of 81 experimentally derived adsorption energies on 12 different transition metals, was also developed recently [12].

These datasets are not only invaluable for DFT benchmarking but also serve as yardsticks for probing the issue of transferability across various available quantum chemistry codes. Since codes employ a diverse range of pseudopotential approximations, or "frozen-core" representations of the core electrons in an atom, the question of reproducibility of DFT performance across codes must be addressed. A recent study demonstrated, based on PBE predictions of a representative bulk property across several codes and pseudopotentials, that the problem of transferability is "solved" [13]. However, it is unlikely that a single bulk structure measure can fully represent all the challenges in preparing a transferable and accurate pseudopotential, especially for applications in surface chemistry.

This paper describes the development of ADS41, a dataset of 41 adsorption energies expanded from the original CE39 dataset to include two adsorption reactions on Pt(111) [14–16]. Section II describes the composition and broad classification of the dataset. Section III analyzes the dependence of lattice constants of the transition metals included in ADS41 and adsorption energies calculated using

*Present address: COMSOL AB, Tegnérgatan 23, 111 40 Stockholm, Sweden.

TABLE I. ADS41: dataset of 26 chemisorption and 15 dispersion-dominated adsorption energies on transition metal surfaces. The mixed systems are labeled with an asterisk (*). The column labeled "Experiment (eV)" corresponds to experimental adsorption energies from which zero-point contributions (calculated using PBE) [9] have been subtracted for direct comparison with DFT results.

Type	Reaction	Experiment (eV)
Chemisorption	$C_2H_4 + Pt(111) \rightarrow CCH_3/Pt(111) + H/Pt(111)$	−1.36
	$CH_2I_2 + Pt(111) \rightarrow CH/Pt(111) + H/Pt(111) + 2I/Pt(111)$	−4.72
	$CH_3I + Pt(111) \rightarrow CH_3/Pt(111) + I/Pt(111)$	−2.17
	$CO + Co(001) \rightarrow CO/Co(001)$	−1.23
	$CO + Cu(111) \rightarrow CO/Cu(111)$	−0.59
	$CO + Ir(111) \rightarrow CO/Ir(111)$	−1.70
	$CO + Ni(111) \rightarrow CO/Ni(111)$	−1.29
	$CO + Pd(100) \rightarrow CO/Pd(100)$	−1.63
	$CO + Pd(111) \rightarrow CO/Pd(111)$	−1.49
	$CO + Pt(111) \rightarrow CO/Pt(111)$	−1.29
	$CO + Rh(111) \rightarrow CO/Rh(111)$	−1.47
	$CO + Ru(001) \rightarrow CO/Ru(001)$	−1.67
	$H_2/Ni(100) \rightarrow 2H/Ni(100)$	−0.90
	$H_2/Ni(111) \rightarrow 2H/Ni(111)$	−1.04
	$H_2/Pd(111) \rightarrow 2H/Pd(111)$	−0.93
	$H_2/Pt(111) \rightarrow 2H/Pt(111)$	−0.75
	$H_2/Rh(111) \rightarrow 2H/Rh(111)$	−0.75
	$I_2/Pt(111) \rightarrow 2I/Pt(111)$	−3.24
	$NO + Ni(100) \rightarrow N/Ni(100) + O/Ni(100)$	−3.10
	$NO + Pd(100) \rightarrow NO/Pd(100)$	−1.69
	$NO + Pd(111) \rightarrow NO/Pd(111)$	−1.89
	$NO + Pt(111) \rightarrow NO/Pt(111)$	−1.23
	$O_2/Ni(100) \rightarrow 2O/Ni(100)$	−5.49
	$O_2/Ni(111) \rightarrow 2O/Ni(111)$	−5.03
	$O_2/Pt(111) \rightarrow 2O/Pt(111)$	−2.16
	$O_2/Rh(100) \rightarrow 2O/Rh(100)$	−3.68
Dispersion	$C_2H_6 + Pt(111) \rightarrow C_2H_6/Pt(111)$	−0.28
	$C_3H_8 + Pt(111) \rightarrow C_3H_8/Pt(111)$	−0.40
	$C_4H_{10} + Pt(111) \rightarrow C_4H_{10}/Pt(111)$	−0.50
	$C_6H_6 + Ag(111) \rightarrow C_6H_6/Ag(111)$*	−0.63
	$C_6H_6 + Au(111) \rightarrow C_6H_6/Au(111)$*	−0.73
	$C_6H_6 + Cu(111) \rightarrow C_6H_6/Cu(111)$*	−0.68
	$C_6H_6 + Pt(111) \rightarrow C_6H_6/Pt(111)$*	−1.68
	$C_6H_{10} + Pt(111) \rightarrow C_6H_{10}/Pt(111)$*	−1.27
	$C_{10}H_8 + Pt(111) \rightarrow C_{10}H_8/Pt(111)$*	−2.76
	$CH_3I + Pt(111) \rightarrow CH_3I/Pt(111)$*	−0.87
	$CH_3OH + Pt(111) \rightarrow CH_3OH/Pt(111)$	−0.57
	$CH_4/Pt(111) \rightarrow CH_4/Pt(111)$	−0.15
	$D_2O + 1/3[O/Pt(111)] \rightarrow 2/3[(D_2O \cdots OD)/Pt(111)]$	−0.68
	$D_2O + Pt(111) \rightarrow D_2O/Pt(111)$	−0.57
	$NH_3/Cu(100) \rightarrow NH_3/Cu(100)$	−0.62

representative functionals on the underlying codes and pseudopotentials. Section IV discusses the accuracies of several density functionals spanning several widely used classes—GGAs, dispersion-corrected GGAs, metaGGAs, dispersion-corrected metaGGAs and screened hybrids in the prediction of adsorption energies. In Sec. V, the implications of these accuracies for predicting activation barriers to dissociation reactions are discussed based on the recent development of a dataset of barrier heights, SBH10 [17], in this group. The final section summarizes the key findings and emphasizes the fact that there is no single functional that can capture the entirety of electronic interactions between the surface of the transition metal and the adsorbate. In this work, we mainly focus on the energetic properties of ADS41 dataset, and the geometric and electronic properties of the dataset will be studied in the future.

II. ADS41: ADSORPTION ENERGIES ON TRANSITION METAL SURFACES

Table I shows the systems comprising the ADS41 dataset, expanded from the previous CE39 dataset [9] of 39 experimental adsorption energies, to include two additional systems reported by Gautier *et al.* [14]—ethylene dissociation (C_2H_4) on Pt(111) to form adsorbed ethylidyne (CCH_3) and hydrogen [15] and naphthalene ($C_{10}H_8$) adsorption on Pt(111) [16].

Adsorption energy references in the ADS41 datasets are based on single-crystal adsorption calorimetry [15,18,19], temperature programmed desorption, and equilibrium adsorbate coverage experiments. The 41 systems fall under two broad categories, "chemisorption" and "dispersion" (or physisorption), based on the dominant interaction between the adsorbate and the transition metal surface. It must be noted that this is a simple classification since some systems classified under dispersion, such as alkenes and aromatics on reactive surfaces like Pt, exhibit a mixture of both covalent and noncovalent interactions. The accuracies of various functionals for these "mixed" systems, namely, benzene (C_6H_6), cyclohexene (C_6H_{10}), and naphthalene ($C_{10}H_8$) on Pt(111), are also addressed in this study.

III. ANALYSIS OF CODE AND PSEUDOPOTENTIAL DEPENDENCE

In a recent study, Lejaeghere *et al.* [13] demonstrated that the bulk properties of solids are relatively insensitive to the underlying quantum chemistry code or pseudopotentials used. While these results are encouraging, they do not guarantee transferability for properties relevant to surface chemistry such as adsorption energies or dissociation barrier heights. The ADS41 dataset serves as the ideal platform for this purpose. While the analysis by Lejaeghere *et al.* [13] was limited to a GGA functional, PBE [20], this study chooses representative functionals constituting the middle and upper rungs of the Jacob's ladder [21]. These include RPBE [22] as the representative GGA, BEEF-vdW [23] as the dispersion-corrected GGA, MS2 [24,25] and SCAN [26] as the representative metaGGA, and SCAN+rVV10 [27] as the representative of dispersion-corrected metaGGA. The transferability of RPBE and BEEF-vdW functionals warrants close examination since the CE39 study demonstrated that they are the most accurate functionals for determining chemisorption energies using the QUANTUM ESPRESSO (QE) [28] package and projected augmented wave (PAW) setups by Adllan and Dal Corso [29].

Lattice constants and adsorption energies are calculated with the following codes and setups: (1) VASP [30–32] with default PAW setups [33,34] and (2) GPAW [35,36] with version 0.9.2 PAW setups.

BEEF-vdW calculations performed with the QE code [28] and PAW potentials by Adllan and Dal Corso [29] show that lattice constants and adsorption energies are very similar to the results generated with VASP. The mean signed errors for BEEF-vdW adsorption energies with QE (0.13 eV) and VASP (0.11 eV) are within 0.02 eV of each other, with identical root-mean-square errors (0.31 eV). Therefore, the discussion of QE is omitted in this study.

A. fcc lattice constants

In the first step, the code/setup dependence of lattice constants of fcc metals constituting ADS41—Rh, Ir, Ni, Pd, Pt, Cu, Ag and Au—is examined. Since ADS41 consists of only two hcp metals, Co and Ru, the analysis of lattice constants does not include trends in hcp metals.

The mean absolute deviations (MADs) associated with deviation of lattice constants of fcc metals from experiment are shown in Fig. 1. The experimental references are identical

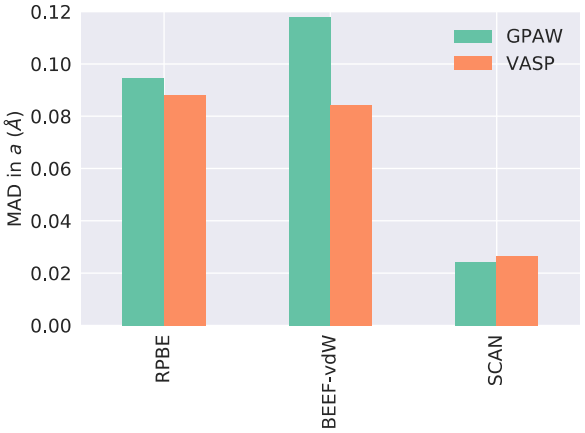

FIG. 1. Mean absolute deviations (MAD) of fcc lattice constants for RPBE, BEEF-vdW, and SCAN calculated using GPAW and VASP, respectively. While the GGA functional RPBE and the metaGGA SCAN MADs agree within 10%, BEEF-vdW MADs are significantly different.

to those employed in the training of the BEEF-vdW functional [23,37]. The MADs for SCAN and RPBE functionals are in good agreement across both codes and pseudopotentials. SCAN lattice constants are more accurate than those calculated with RPBE or BEEF-vdW, as demonstrated in another recent study [38]. However, the MAD for BEEF-vdW with GPAW is over 30% worse than with VASP, while the errors differ by less than 10% for RPBE and SCAN functionals.

B. Adsorption energies

Figure 2 depicts MADs for calculated chemisorption [Fig. 2(a)] and dispersion [Fig. 2(b)] energies. Chemisorption energy errors across GPAW and VASP differ by less than 0.1 eV for all functionals. The observed differences in RPBE errors between GPAW and VASP stem mainly from CO chemisorption systems, where GPAW overbinds CO in every system by about 0.2 eV. We hypothesize that this discrepancy potentially stems from a poor description of the gas phase reference in

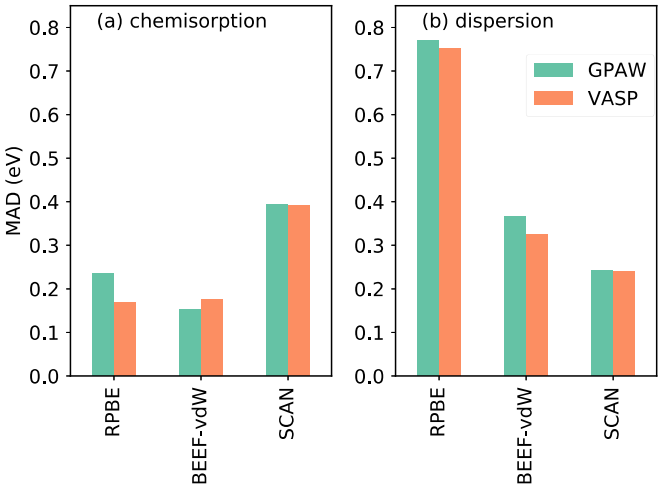

FIG. 2. Mean absolute deviations in (a) chemisorption energies and (b) dispersion energies for RPBE, BEEF-vdW, and SCAN functionals calculated using GPAW and VASP codes.

GPAW. However, further investigation is required since CO chemisorption energy differences between VASP and GPAW are negligible with the BEEF-vdW and SCAN functionals. It must also be noted that while BEEF-vdW lattice constants are sensitive to the underlying code, as shown in Fig. 1, these differences appear to cancel out during the calculation of chemisorption energies.

MADs for dispersion-dominated systems calculating with RPBE and SCAN functionals are very similar with GPAW and VASP. The only exceptions with RPBE are benzene and naphthalene adsorption on Pt(111). In both cases, GPAW underbinds by about 0.25 eV when compared to VASP. The largest difference in MAD in dispersion-dominated systems is observed with BEEF-vdW, where GPAW underbinds benzene, naphthalene, and CH_3I on Pt(111) by 0.47, 0.22, and 0.13 eV, respectively.

This analysis demonstrates that lattice constants with the BEEF-vdW are code specific, but with a few exceptions, these errors cancel out in the estimation of adsorption energies. One reason for the higher sensitivity of BEEF-vdW compared to RPBE or SCAN is the fact that the vdW-DF2 correction is sensitive to the pseudopotentials used. In all codes considered here (GPAW, VASP, and QUANTUM ESPRESSO), vdW-DF terms are calculated from the pseudo density only; neither core nor augmentation corrections are applied. Hence, the vdW terms spuriously depend on both the hardness and the valency of the pseudopotentials. In addition, the BEEF fitting procedure, which aims to minimize functional errors within the framework of a single code and its pseudopotentials, will provide the most accurate functional for that framework. As a result, the functional parameters optimized for densities calculated using a particular set of pseudopotentials may not demonstrate identical accuracies for a different code or pseudopotentials. Herein, we have identified one of the key limitations of Bayesian error estimation functionals. The BEEF methodology will produce the most accurate functional for a certain reference dataset on a specific rung of Jacob's ladder but will do so mainly within one specific code and set of pseudopotentials.

IV. ADSORPTION ON TRANSITION METAL SURFACES: BENCHMARKING DFT

Representative functionals from rungs 2 to 4 of Jacob's ladder [21] of density functional approximations are chosen for benchmarking DFT performance—(1) GGA: PBE [20] and RPBE [22], (2) GGA-vdW: optPBE-vdW [39] and BEEF-vdW [23], (3) metaGGA: MS2 [24,25], SCAN [26], and SCAN+rVV10 [40], and (4) short-range screened hybrid: HSE06 [41].

The benchmarking calculations are performed using the VASP 5.3.5 package. The details of model setup and calculations are described in Appendixes A and B. The adsorption energies are listed in Table II, and the corresponding errors, calculated on a per adsorbate basis, are shown in Table III. All structures and energies generated in this work are available in the SUNCAT Catalysis Hub databse located at https://www.catalysis-hub.org/publications/SharadaAdsorption2019 [42].

A. GGA

Figures 3(a) and 3(b) show GGA adsorption energy errors for chemisorption and dispersion-dominated systems, respectively. The relative accuracies of the PBE and RPBE functionals are discussed in detail in the previous CE39 study [9]. In general, RPBE is the GGA of choice for studying chemisorption on transition metal surfaces since it is designed specifically to overcome the problem of excessive binding with the PBE functional. Since GGAs do not include nonlocal correlation or van der Waals (vdW) terms within their exchange-correlation formalism, the dispersion-bound systems, unsurprisingly, are poorly described by PBE and RPBE. For systems consisting of mixed covalent and dispersion interactions—C_6H_6, C_6H_{10}, and $C_{10}H_8$ on Pt(111)—RPBE deviates more strongly from experiment compared to PBE. It is possible that the overbinding tendency of PBE partially compensates for the functional's inability to capture these interactions, leading to smaller errors for mixed systems.

B. Dispersion-corrected GGA

As demonstrated in the CE39 study [9], a dispersion-corrected GGA such as BEEF-vdW improves the prediction of adsorption energies for dispersion-dominated interactions between the adsorbate and surface. The benchmarking is extended to an additional dispersion-corrected GGA, optPBE-vdW, which is styled along the lines of PBE and includes the self-consistently determined vdW-DF1 correction [43]. BEEF-vdW is a Bayesian error estimation functional [44] developed using a Bayesian approach for fitting exchange-correlation parameters to properties relevant to surface chemistry. BEEF-vdW employs the self-consistent vdW-DF2 approximation for capturing dispersion interactions [45].

Figure 4 describes the errors in adsorption energies for optPBE-vdW and BEEF-vdW. While the latter demonstrates chemisorption accuracies comparable to RPBE, with a root-mean-square deviation (RMSD) of 0.21 eV, optPBE-vdW exhibits significant overbinding, with mean signed deviation (MSD) of −0.41 eV and RMSD 0.54 eV. Since the tendency to overbind is stronger with optPBE-vdW relative to PBE (Fig. 3), it is possible that the errors stem from larger dispersion corrections caused by larger C_6 coefficients in the vdW-DF1 approximation (relative to vdW-DF2) [46]. On the other hand, optPBE-vdW yields some of the lowest errors across all benchmarked functionals for dispersion-dominated as well as mixed adsorption systems, which was also demonstrated recently by Gautier *et al.* [14] for adsorption on Pt(111).

BEEF-vdW yields very low chemisorption errors since the functional has been trained on a dataset consisting of 17 chemisorption energies (CE17) [23]. However, as pointed out in the CE39 benchmarking study, BEEF-vdW systematically underestimates binding for the vdW systems [9], with errors for mixed systems comparable to the PBE functional [14]. The exact origin of the tendency of BEEF-vdW to underestimate dispersion-dominated binding is not known since these errors can stem from a combination of factors, including poor description of aromatic systems or the absence of dispersion-dominated adsorption in the BEEF-vdW training data. It is hypothesized that including dispersion-dominated adsorption

TABLE II. DFT adsorption energies (eV) for systems constituting the ADS41 dataset.

Type	Reaction	Expt	PBE	RPBE	optPBE-vdW	BEEF-vdW	MS2	SCAN	SCAN+rVV10	HSE06
Chemisorption	$C_2H_4 + Pt(111) \rightarrow CCH_3/Pt(111) + H/Pt(111)$	−1.36	−1.65	−1.20	−1.83	−1.34	−1.68	−2.21	−2.33	−2.21
	$CH_2I_2 + Pt(111) \rightarrow CH/Pt(111) + H/Pt(111) + 2I/Pt(111)$	−4.72	−3.85	−3.05	−4.27	−3.47	−3.70	−4.88	−5.27	−4.81
	$CH_3I + Pt(111) \rightarrow CH_3/Pt(111) + I/Pt(111)$	−2.17	−1.66	−1.22	−2.12	−1.68	−1.76	−2.36	−2.63	−1.98
	$CO + Co(001) \rightarrow CO/Co(001)$	−1.23	−1.63	−1.33	−1.71	−1.40	−1.32	−1.72	−1.82	−1.52
	$CO + Cu(111) \rightarrow CO/Cu(111)$	−0.59	−0.75	−0.48	−0.78	−0.51	−0.67	−0.91	−0.99	−0.56
	$CO + Ir(111) \rightarrow CO/Ir(111)$	−1.70	−1.93	−1.67	−2.03	−1.78	−1.84	−2.04	−2.14	−2.43
	$CO + Ni(111) \rightarrow CO/Ni(111)$	−1.29	−1.81	−1.42	−1.93	−1.57	−1.49	−1.88	−2.00	−1.09
	$CO + Pd(100) \rightarrow CO/Pd(100)$	−1.63	−1.86	−1.52	−1.94	−1.61	−1.86	−2.09	−2.20	−1.99
	$CO + Pd(111) \rightarrow CO/Pd(111)$	−1.49	−1.95	−1.58	−2.08	−1.74	−1.95	−2.19	−2.30	−2.15
	$CO + Pt(111) \rightarrow CO/Pt(111)$	−1.29	−1.64	−1.36	−1.68	−1.39	−1.49	−1.94	−2.02	−1.72
	$CO + Rh(111) \rightarrow CO/Rh(111)$	−1.47	−1.84	−1.57	−1.96	−1.68	−1.82	−2.04	−2.14	−2.23
	$CO + Ru(001) \rightarrow CO/Ru(001)$	−1.67	−1.88	−1.61	−1.96	−1.71	−1.82	−1.95	−2.05	−1.99
	$H_2/Ni(100) \rightarrow 2H/Ni(100)$	−0.90	−1.01	−0.65	−0.90	−0.58	−1.19	−1.29	−1.13	−0.66
	$H_2/Ni(111) \rightarrow 2H/Ni(111)$	−1.04	−1.10	−0.77	−1.05	−0.69	−1.28	−1.28	−1.30	−1.26
	$H_2/Pd(111) \rightarrow 2H/Pd(111)$	−0.93	−1.20	−0.88	−1.10	−0.73	−1.40	−1.44	−1.46	−1.45
	$H_2/Pt(111) \rightarrow 2H/Pt(111)$	−0.75	−0.96	−0.65	−0.79	−0.47	−0.86	−1.11	−1.12	−1.22
	$H_2/Rh(111) \rightarrow 2H/Rh(111)$	−0.75	−1.07	−0.76	−0.91	−0.56	−1.20	−1.22	−1.25	−1.45
	$I_2/Pt(111) \rightarrow 2I/Pt(111)$	−3.24	−2.84	−2.27	−3.28	−2.78	−2.99	−3.49	−3.81	−3.37
	$NO + Ni(100) \rightarrow N/Ni(100) + O/Ni(100)$	−3.10	−4.37	−3.72	−5.27	−3.99	−4.27	−5.00	−5.13	−4.01
	$NO + Pd(100) \rightarrow NO/Pd(100)$	−1.69	−2.05	−1.63	−2.60	−1.82	−2.02	−2.19	−2.32	−1.94
	$NO + Pd(111) \rightarrow NO/Pd(111)$	−1.89	−2.23	−1.83	−2.80	−2.07	−2.18	−2.37	−2.48	−2.17
	$NO + Pt(111) \rightarrow NO/Pt(111)$	−1.23	−1.83	−1.43	−2.23	−1.52	−1.46	−1.91	−2.01	−1.80
	$O_2/Ni(100) \rightarrow 2O/Ni(100)$	−5.49	−5.07	−4.50	−6.66	−4.92	−5.18	−6.19	−6.29	−4.79
	$O_2/Ni(111) \rightarrow 2O/Ni(111)$	−5.03	−4.58	−4.08	−6.12	−4.37	−4.48	−5.24	−5.34	−3.94
	$O_2/Pt(111) \rightarrow 2O/Pt(111)$	−2.16	−2.37	−1.86	−3.20	−2.10	−2.43	−2.91	−2.94	−2.32
	$O_2/Rh(100) \rightarrow 2O/Rh(100)$	−3.68	−4.33	−3.76	−5.79	−4.03	−4.82	−4.92	−5.05	−5.00
Dispersion	$C_2H_6 + Pt(111) \rightarrow C_2H_6/Pt(111)$	−0.28	−0.04	−0.02	−0.35	−0.22	−0.07	−0.14	−0.27	−0.02
	$C_3H_8 + Pt(111) \rightarrow C_3H_8/Pt(111)$	−0.40	−0.05	−0.01	−0.48	−0.30	−0.10	−0.20	−0.39	−0.06
	$C_4H_{10} + Pt(111) \rightarrow C_4H_{10}/Pt(111)$	−0.50	−0.07	−0.02	−0.62	−0.41	−0.13	−0.27	−0.68	−0.04
	$C_6H_6 + Ag(111) \rightarrow C_6H_6/Ag(111)^*$	−0.63	−0.05	0.00	−0.67	−0.32	−0.22	−0.27	−0.67	0.07
	$C_6H_6 + Au(111) \rightarrow C_6H_6/Au(111)^*$	−0.73	−0.05	−0.01	−0.76	−0.41	−0.26	−0.38	−0.72	0.18
	$C_6H_6 + Cu(111) \rightarrow C_6H_6/Cu(111)^*$	−0.68	−0.05	0.00	−0.74	−0.41	−0.27	−0.30	−0.70	0.08
	$C_6H_6 + Pt(111) \rightarrow C_6H_6/Pt(111)^*$	−1.68	−0.98	−0.17	−1.80	−0.93	−1.59	−1.94	−2.41	−1.53
	$C_6H_{10} + Pt(111) \rightarrow C_6H_{10}/Pt(111)^*$	−1.27	−0.63	−0.07	−1.55	−0.81	−0.95	−1.38	−1.81	−0.80
	$C_{10}H_8 + Pt(111) \rightarrow C_{10}H_8/Pt(111)^*$	−2.76	−1.84	−0.08	−2.76	−1.59	−2.58	−3.27	−2.35	−2.86
	$CH_3I + Pt(111) \rightarrow CH_3I/Pt(111)^*$	−0.87	−0.25	0.00	−0.71	−0.41	−0.34	−0.39	−0.61	−0.25
	$CH_3OH + Pt(111) \rightarrow CH_3OH/Pt(111)$	−0.57	−0.21	−0.05	−0.64	−0.34	−0.33	−0.73	−0.89	−0.17
	$CH_4/Pt(111) \rightarrow CH_4/Pt(111)$	−0.15	−0.02	−0.01	−0.21	−0.15	−0.04	−0.08	−0.16	0.02
	$D_2O + 1/3[O/Pt(111)] \rightarrow 2/3[(D_2O \cdots OD)/Pt(111)]$	−0.68	−0.66	−0.19	−1.20	−0.61	−0.91	−1.13	−1.31	−0.75
	$D_2O + Pt(111) \rightarrow D_2O/Pt(111)$	−0.57	−0.21	−0.05	−0.39	−0.22	−0.09	−0.66	−0.75	−0.19
	$NH_3/Cu(100) \rightarrow NH_3/Cu(100)$	−0.62	−0.43	−0.21	−0.60	−0.39	−0.46	−0.58	−0.69	−0.36

TABLE III. DFT errors adsorption energies (eV) for systems constituting the ADS41 dataset. All errors are scaled by the number of adsorbates. Overall error statistics (eV) are also reported.

Type	Reaction	PBE	RPBE	optPBE-vdW	BEEF-vdW	MS2	SCAN	SCAN+rVV10	HSE06
Chemisorption	$C_2H_4 + Pt(111) \rightarrow CCH_3/Pt(111) + H/Pt(111)$	−0.15	0.08	−0.24	0.01	−0.16	−0.42	−0.48	−0.42
	$CH_2I_2 + Pt(111) \rightarrow CH/Pt(111) + H/Pt(111) + 2I/Pt(111)$	0.22	0.42	0.11	0.31	0.25	−0.04	−0.14	−0.02
	$CH_3I + Pt(111) \rightarrow CH_3/Pt(111) + I/Pt(111)$	0.25	0.48	0.02	0.24	0.20	−0.10	−0.23	0.09
	$CO + Co(001) \rightarrow CO/Co(001)$	−0.40	−0.10	−0.48	−0.17	−0.09	−0.49	−0.59	−0.29
	$CO + Cu(111) \rightarrow CO/Cu(111)$	−0.16	0.11	−0.19	0.08	−0.08	−0.32	−0.40	0.03
	$CO + Ir(111) \rightarrow CO/Ir(111)$	−0.23	0.03	−0.33	−0.08	−0.14	−0.34	−0.44	−0.73
	$CO + Ni(111) \rightarrow CO/Ni(111)$	−0.52	−0.13	−0.64	−0.29	−0.21	−0.60	−0.71	0.20
	$CO + Pd(100) \rightarrow CO/Pd(100)$	−0.23	0.11	−0.31	0.01	−0.23	−0.47	−0.57	−0.36
	$CO + Pd(111) \rightarrow CO/Pd(111)$	−0.46	−0.09	−0.59	−0.25	−0.45	−0.70	−0.81	−0.66
	$CO + Pt(111) \rightarrow CO/Pt(111)$	−0.36	−0.08	−0.39	−0.11	−0.21	−0.65	−0.74	−0.43
	$CO + Rh(111) \rightarrow CO/Rh(111)$	−0.37	−0.10	−0.49	−0.21	−0.34	−0.57	−0.67	−0.76
	$CO + Ru(001) \rightarrow CO/Ru(001)$	−0.21	0.06	−0.29	−0.04	−0.15	−0.29	−0.38	−0.32
	$H_2/Ni(100) \rightarrow 2H/Ni(100)$	−0.05	0.12	0.00	0.16	−0.14	−0.19	−0.12	0.12
	$H_2/Ni(111) \rightarrow 2H/Ni(111)$	−0.03	0.13	−0.01	0.18	−0.12	−0.12	−0.13	−0.11
	$H_2/Pd(111) \rightarrow 2H/Pd(111)$	−0.13	0.03	−0.09	0.10	−0.23	−0.25	−0.26	−0.26
	$H_2/Pt(111) \rightarrow 2H/Pt(111)$	−0.11	0.05	−0.02	0.14	−0.06	−0.18	−0.19	−0.24
	$H_2/Rh(111) \rightarrow 2H/Rh(111)$	−0.16	−0.01	−0.08	0.09	−0.23	−0.24	−0.25	−0.35
	$I_2/Pt(111) \rightarrow 2I/Pt(111)$	0.20	0.49	−0.02	0.23	0.13	−0.12	−0.28	−0.06
	$NO + Ni(100) \rightarrow N/Ni(100) + O/Ni(100)$	−0.64	−0.31	−1.08	−0.44	−0.59	−0.95	−1.01	−0.46
	$NO + Pd(100) \rightarrow NO/Pd(100)$	−0.36	0.06	−0.91	−0.13	−0.33	−0.50	−0.63	−0.25
	$NO + Pd(111) \rightarrow NO/Pd(111)$	−0.34	0.05	−0.91	−0.18	−0.29	−0.48	−0.59	−0.29
	$NO + Pt(111) \rightarrow NO/Pt(111)$	−0.59	−0.20	−1.00	−0.29	−0.23	−0.67	−0.78	−0.57
	$O_2/Ni(100) \rightarrow 2O/Ni(100)$	0.21	0.50	−0.58	0.29	0.16	−0.35	−0.40	0.35
	$O_2/Ni(111) \rightarrow 2O/Ni(111)$	0.22	0.47	−0.55	0.33	0.27	−0.11	−0.16	0.55
	$O_2/Pt(111) \rightarrow 2O/Pt(111)$	−0.11	0.15	−0.52	0.03	−0.13	−0.38	−0.39	−0.08
	$O_2/Rh(100) \rightarrow 2O/Rh(100)$	−0.33	−0.04	−1.06	−0.17	−0.57	−0.62	−0.69	−0.66
Dispersion	$C_2H_6 + Pt(111) \rightarrow C_2H_6/Pt(111)$	0.24	0.26	−0.07	0.06	0.21	0.14	0.01	0.26
	$C_3H_8 + Pt(111) \rightarrow C_3H_8/Pt(111)$	0.35	0.39	−0.07	0.10	0.31	0.20	0.02	0.34
	$C_4H_{10} + Pt(111) \rightarrow C_4H_{10}/Pt(111)$	0.43	0.48	−0.12	0.09	0.36	0.22	−0.18	0.46
	$C_6H_6 + Ag(111) \rightarrow C_6H_6/Ag(111)$*	0.59	0.63	−0.04	0.32	0.41	0.36	−0.03	0.70
	$C_6H_6 + Au(111) \rightarrow C_6H_6/Au(111)$*	0.67	0.72	−0.03	0.32	0.46	0.35	0.01	0.90
	$C_6H_6 + Cu(111) \rightarrow C_6H_6/Cu(111)$*	0.64	0.69	−0.05	0.27	0.41	0.38	−0.01	0.77
	$C_6H_6 + Pt(111) \rightarrow C_6H_6/Pt(111)$*	0.70	1.51	−0.13	0.75	0.09	−0.26	−0.73	0.15
	$C_6H_{10} + Pt(111) \rightarrow C_6H_{10}/Pt(111)$*	0.65	1.20	−0.27	0.46	0.33	−0.11	−0.53	0.47
	$C_{10}H_8 + Pt(111) \rightarrow C_{10}H_8/Pt(111)$*	0.93	2.69	0.01	1.17	0.18	−0.50	0.41	−0.10
	$CH_3I + Pt(111) \rightarrow CH_3I/Pt(111)$*	0.62	0.87	0.16	0.46	0.53	0.48	0.27	0.62
	$CH_3OH + Pt(111) \rightarrow CH_3OH/Pt(111)$	0.36	0.52	−0.07	0.23	0.24	−0.16	−0.32	0.40
	$CH_4/Pt(111) \rightarrow CH_4/Pt(111)$	0.13	0.13	−0.07	−0.01	0.10	0.07	−0.02	0.17
	$D_2O + 1/3[O/Pt(111)] \rightarrow 2/3[(D_2O \cdots OD)/Pt(111)]$	0.01	0.26	−0.28	0.04	−0.12	−0.24	−0.34	−0.03
	$D_2O + Pt(111) \rightarrow D_2O/Pt(111)$	0.36	0.52	0.18	0.35	0.48	−0.09	−0.18	0.38
	$NH_3/Cu(100) \rightarrow NH_3/Cu(100)$	0.19	0.41	0.02	0.23	0.17	0.04	−0.07	0.26
Error statistics	Mean signed deviation (MSD)	0.05	0.33	−0.28	0.11	0.00	−0.23	−0.33	−0.01
	Mean absolute deviation (MAD)	0.34	0.38	0.30	0.23	0.25	0.34	0.37	0.36
	Root mean square deviation (RMSD)	0.40	0.62	0.44	0.31	0.29	0.40	0.45	0.43

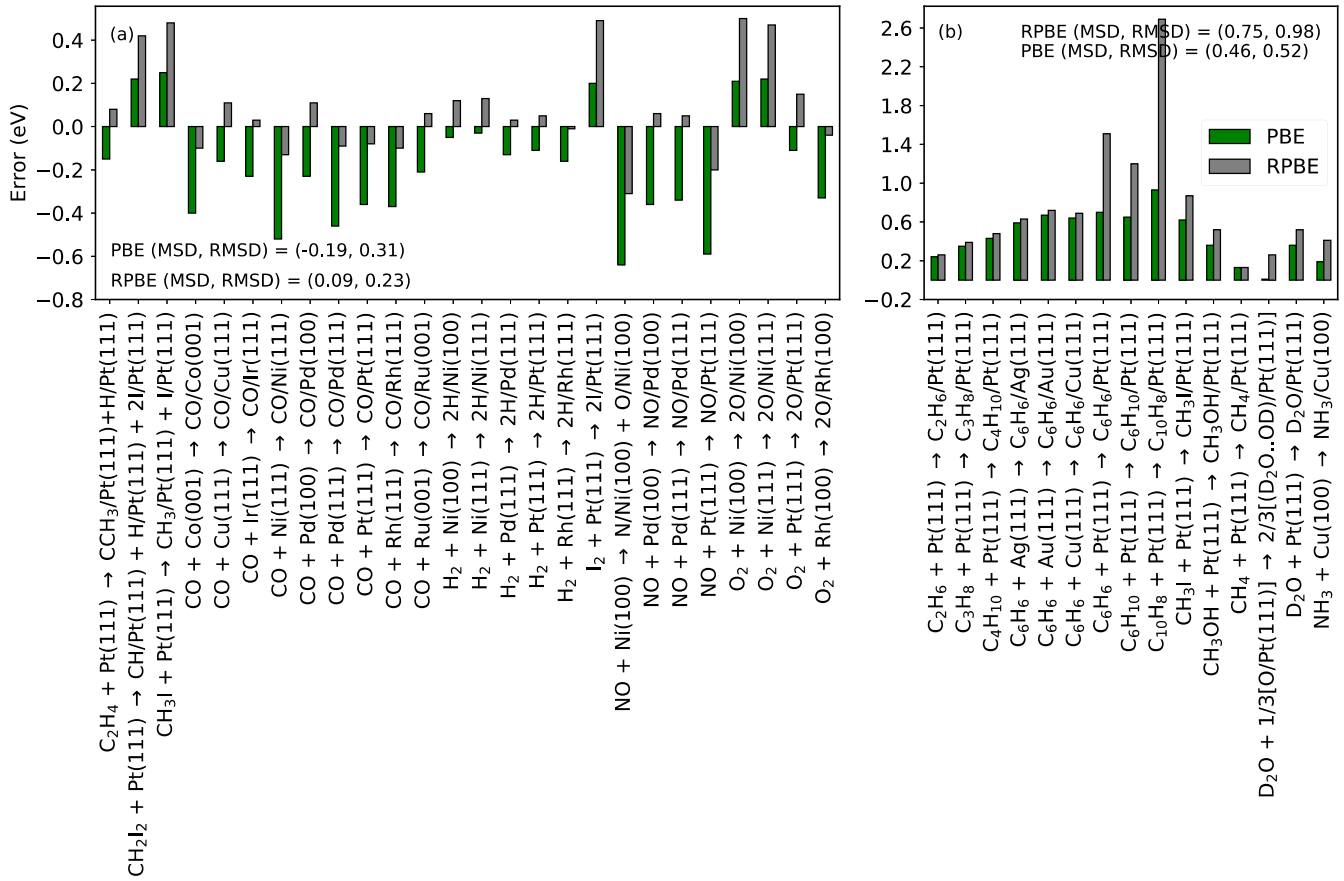

FIG. 3. GGAs: Comparison between PBE and RPBE errors (eV) for (a) chemisorption and (b) dispersion-dominated systems in the ADS41 dataset.

systems in the training dataset for future iterations of Bayesian error estimation functionals will aid in improving accuracies.

C. metaGGA and dispersion-corrected metaGGA

Prior studies have shown that some metaGGAs can accurately describe adsorption on transition metal surfaces. Garza *et al.* suggested that the RTPSS functional can be useful for studying the chemisorption processes [47]. By generalizing DFT-D3 across widely used density functionals, Witte *et al.* found that the revPBE0-D3(op) and MS2-D3(op) methods reduce errors associated with noncovalent interaction energies and geometries [48]. The metaGGA functionals, including surface-asymptotics (SA)-TPSS [49], balanced localization (BLOC) metaGGA [50], and the TM functional [51], were proposed as promising methods which improve the accuracy of various properties of molecules, solids, and solid surfaces. The metaGGA variants of Bayesian error estimation functionals, mBEEF [52] and mBEEF-vdW (mBEEF with a vdW-DF2 dispersion correction) [53] for GPAW, were developed recently in this group. Both functionals were trained, among other properties, on chemisorption energies. Therefore, they can predict chemisorption energies in the CE27 dataset [23] to within 0.25 eV. The Minnesota metaGGA M06-L [54] also exhibits accuracies comparable to BEEF-vdW for the CE39 dataset, with the RMS error being only 0.05 eV higher than for BEEF-vdW [10].

The metaGGAs chosen in the current benchmarking study are MS2, SCAN, and SCAN+rVV10. While MS2 is designed to distinguish between various kinds of interactions (covalent, weak, metallic), SCAN is developed based on the satisfaction of all known exact constraints for metaGGAs. SCAN+rVV10 is constructed by supplementing SCAN with the long-range vdW interaction from rVV10 [40]. The errors are contrasted in Fig. 5. Although these functionals tend to overbind, MS2 predicts chemisorption energies with accuracies comparable to RPBE and BEEF-vdW. For nearly all systems, SCAN and SCAN+rVV10 strongly overbind with MSDs that are 0.23 and 0.33 eV more negative than MS2, respectively. Patra *et al.* found that SCAN overbinds CO on transition metal surfaces and explained that the error is due to density-driven self-interaction errors associated with incorrect charge transfer between the molecule and metal surface [55].

Owing to the absence of explicit dispersion corrections in these functionals, MS2 and SCAN exhibit positive errors, in general, for dispersion-bound systems. As a consequence of its tendency to overbind, errors with the SCAN functional are slightly lower than MS2. While MS2 underbinds the mixed systems as well, SCAN exhibits varying degrees of overbinding, with the largest errors for naphthalene adsorption on Pt(111). Although SCAN+rVV10 overbinds most of the chemisorbed systems and some dispersion systems, including benzene and C_6H_{10} on Pt(111), it yields a very small error for the small alkane/alkene adsorption and benzene on coinage

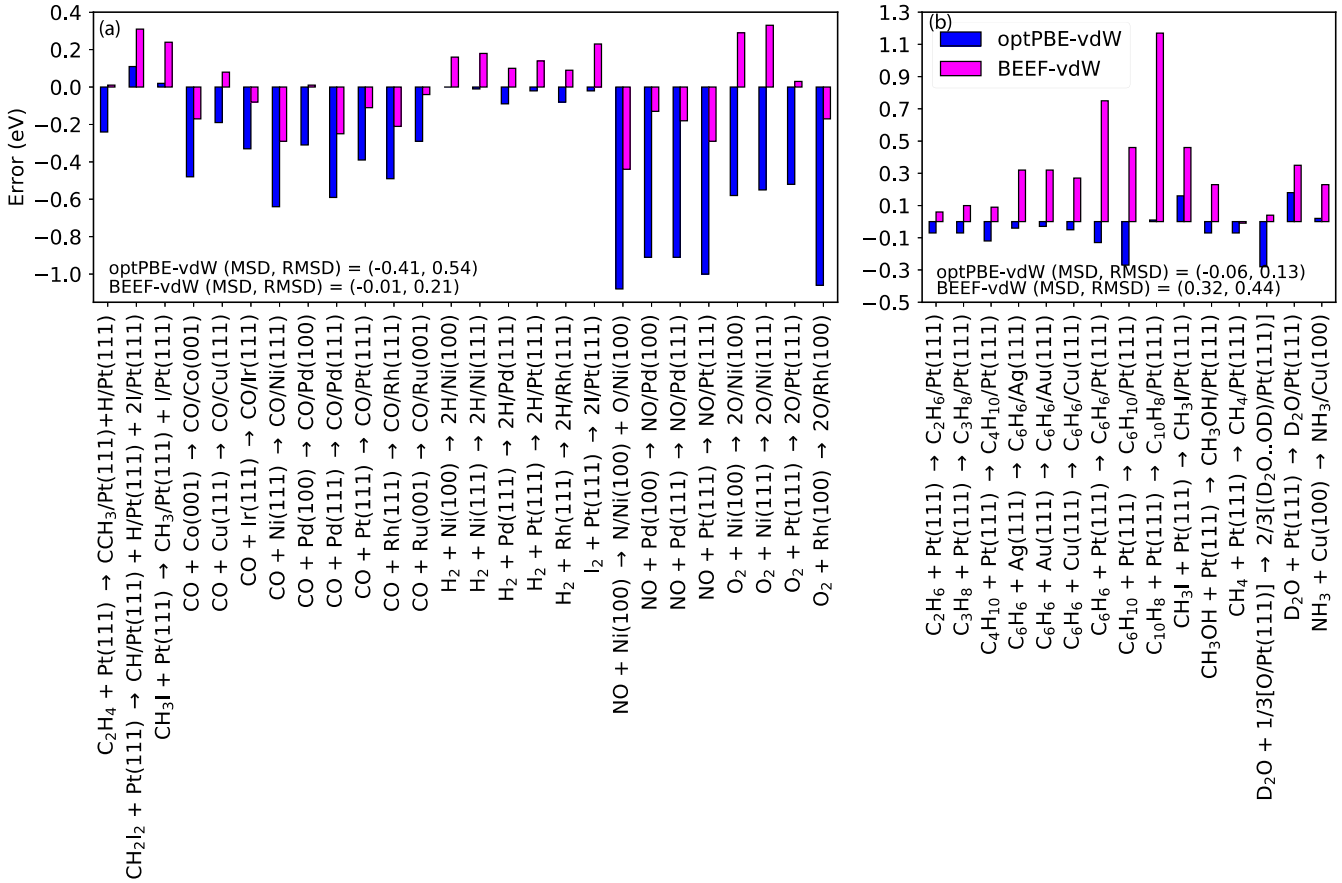

FIG. 4. Dispersion-corrected GGAs: Comparison between optPBE-vdW and BEEF-vdW errors (eV) for (a) chemisorption and (b) dispersion-dominated systems in the ADS41 dataset.

(Ag, Au, Cu) metals. Peng *et al.* [27] demonstrated that this functional accurately describes benzene physisorption on coinage metals and SCAN underestimates binding energies for these systems, which are consistent with our results.

The errors indicate that including a dispersion correction to a metaGGA like MS2 will significantly improve the functional's accuracies in describing both covalently and noncovalently bound systems on transition metal surfaces. SCAN and SCAN+rVV10 systematically overestimate binding between the surface and adsorbate, especially for chemisorbed systems.

D. Short-range screened hybrid

Surface chemistry studies with hybrid and screened hybrid functionals are limited owing to the high cost of calculating the Hartree-Fock exchange. The PBE0 hybrid and HSE03 screened hybrid have shown some promise for surface chemistry. The "CO puzzle" [56] describes the tendency of GGAs to excessively delocalize electrons and consequently predict the highly coordinated fcc site as the preferred site for CO adsorption on transition metals, while experiments predict the top site. PBE0 and HSE06 predict the correct binding site for CO adsorption on Cu and Rh [57] surfaces since they lower the extent of electron delocalization predicted by GGAs [58]. However, much like simple GGAs (PBE), these functionals tend to overbind CO on transition metals [59].

In order to examine whether these observations can be extended to adsorbates other than CO, HSE06 adsorption energies are compared with PBE in Fig. 6. While HSE06 binds H, O, and CO stronger than PBE, NO chemisorption errors are very similar between the two functionals. Systems adsorbing on Ni are anomalous, possibly due to the fact that, unlike GGA or metaGGA functionals, the HSE06 bulk density of states (DOS) for Ni erroneously shows very low electron density close to the Fermi level and saturated magnetic moment, as shown in Fig. 7. Insufficient screening of exchange interactions will likely pose a general problem for the description of chemistry on magnetic transition metal surfaces. For dispersion-bound systems, owing to the absence of an explicit vdW correction, HSE06 errors are nearly identical to those of PBE, as shown in Fig. 6. Hybrid functionals are not advised when computing electronic-structure-based descriptors for transition metal materials because of their poor treatment of static correlation [60]. In our previous study, we showed that HSE06 is outperformed by BEEF-vdW for the ten surface barrier heights for dissociation of small molecules, SBH10 [17]. Therefore, including short-range exact exchange does not necessarily improve the energetics of surface-adsorbate interactions on transition metal surfaces.

Therefore, the inclusion of screened exact exchange does not improve adsorption energy predictions. However, unlike RPBE or the BEEF family, the HSE06 functional was not designed for surface chemistry. In other words, the parameters

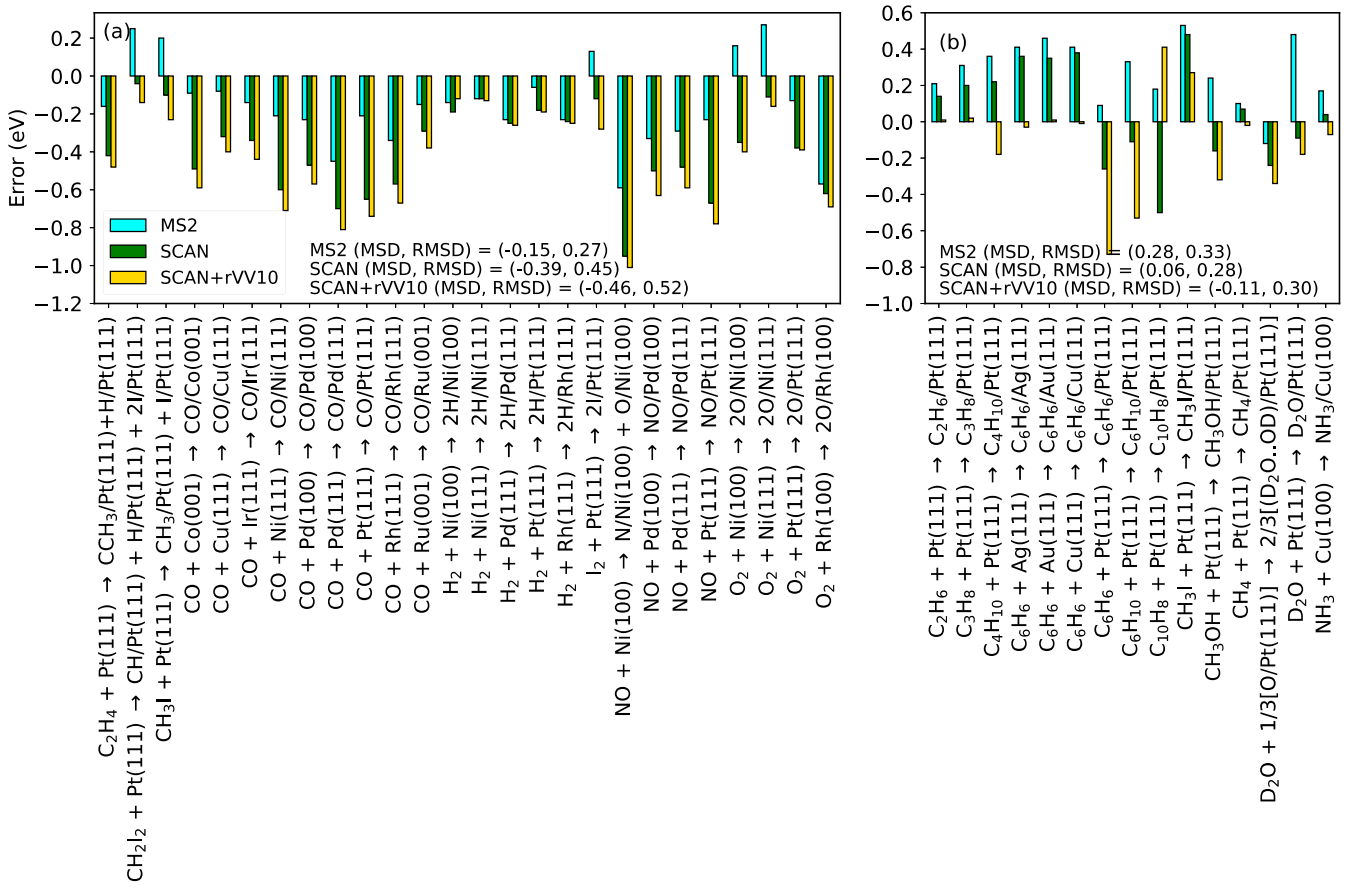

FIG. 5. metaGGAs: Comparison between MS2, SCAN, and SCAN+rVV10 errors (eV) for (a) chemisorption and (b) dispersion-dominated systems in the ADS41 dataset.

controlling the range and fraction of exact exchange are not optimized to treat adsorption. While this study shows that reasonable accuracies can be achieved with computationally less expensive GGA-vdW or metaGGA functionals, exact exchange promises to improve the physical description of surface-adsorbate interactions, as illustrated by the identification of correct CO binding sites on certain transition metals [57]. We believe that it is possible to design a hybrid functional, along the lines of Bayesian error estimation functionals, which can not only be trained on adsorption systems but also help tackle the CO puzzle [56].

V. IMPLICATIONS FOR REACTION KINETICS ON SURFACES

A benchmark dataset of ten apparent barrier heights for the dissociation of small molecules on transition metal surfaces (SBH10), carefully chosen from molecular beam, laser-assisted associative desorption, and thermal rate experiments was recently developed within this group [17]. By comparing BEEF-vdW, MS2, and HSE06 barrier heights, the study demonstrates that a functional that predicts chemisorption energies accurately can also predict barrier heights with comparable accuracies. The reason for this correlation between barrier height and chemisorption energy accuracies is that transition states for dissociation of small molecules on transition metal surfaces closely resemble their respective final states. As a result, a functional that can accurately describe surface-adsorbate interactions in a chemisorbed system can also predict apparent barriers accurately. Since there is little overlap between SBH10 and ADS41, the study illustrates these correlations for dissociative chemisorption reactions of H alone. Therefore, although average MS2 chemisorption errors are comparable to BEEF-vdW, MS2 overbinds H and therefore tends to underestimate barrier heights.

Based on these conclusions, for the dissociation reactions of small molecules—C_2H_4, CH_2I_2, CH_3I, H_2, NO, and O_2 examined in the current study—it is possible to predict whether or not a functional is reliable for kinetics studies. For instance, RPBE not only demonstrates low RMS errors for chemisorption (0.25 eV) but also exhibits errors similar to BEEF-vdW for adsorbates such as H. Therefore, it is safe to say that RPBE can predict barrier heights with accuracies similar to BEEF-vdW for the dissociation of small molecules. Along the same lines, since SCAN binds chemisorbed systems stronger than MS2, the functional will overbind transition states as well, leading to barrier height estimates that are worse than MS2.

VI. CONCLUSIONS

The benchmarking study demonstrates that there are no systematic trends in adsorption energy accuracies across various rungs of density functionals. This is illustrated in Fig. 8, which summarizes the error statistics across all functionals.

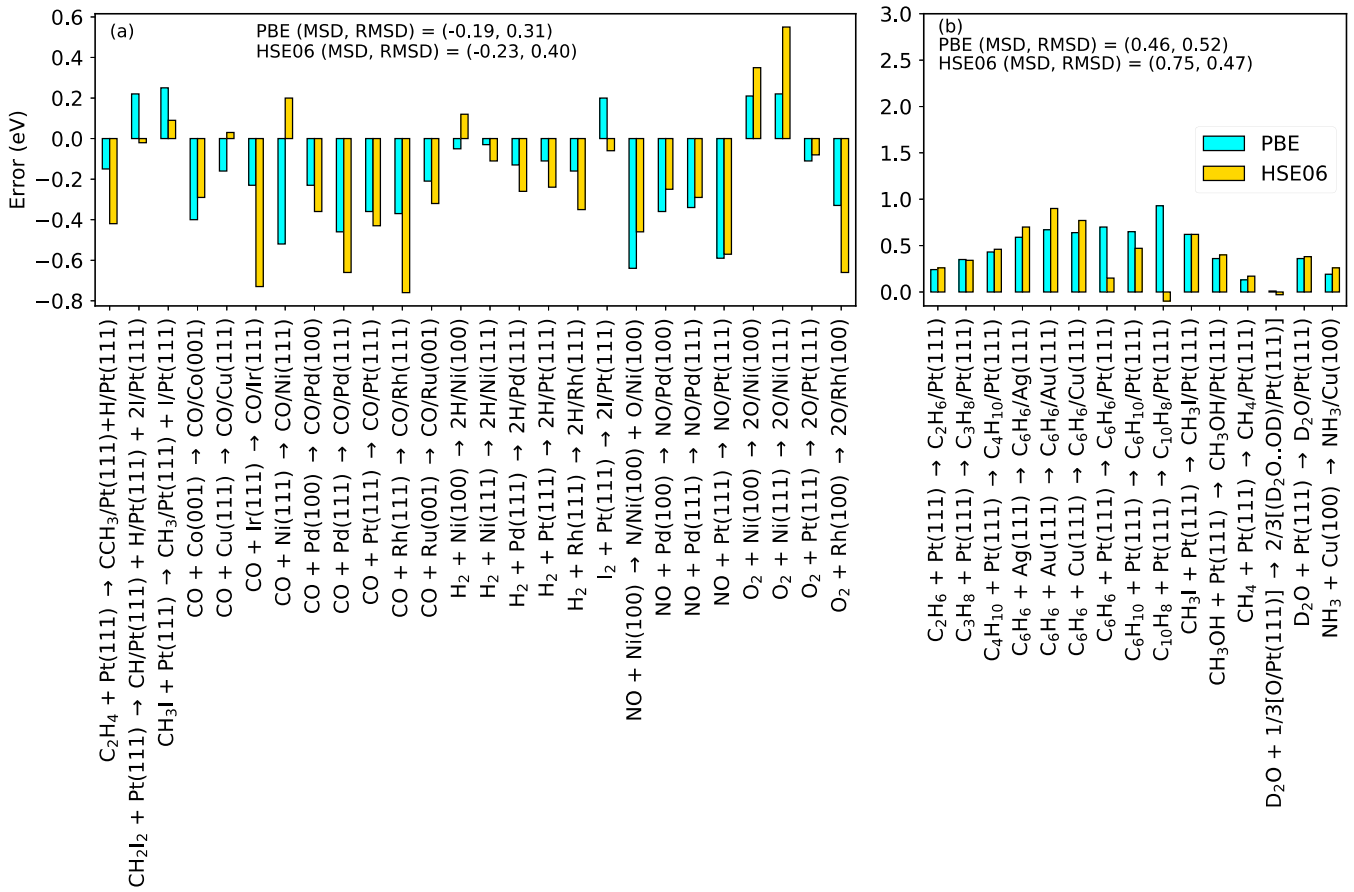

FIG. 6. Screened hybrid: Comparison of HSE06 and the PBE GGA errors (eV) for (a) chemisorption and (b) dispersion-dominated systems in the ADS41 dataset.

Although some GGAs like RPBE are useful for studying chemisorption, they can be erroneous for large or physisorbed adsorbates. Including a dispersion correction can partially remedy this situation, but one runs the risk of overbinding chemisorbed systems, as seen in the case of optPBE-vdW. Therefore, a dispersion-corrected GGA must be chosen with utmost care. As shown in Fig. 8(c) and Table III, MS2 and BEEF-vdW functionals offer the most reliable compromise between describing covalent, noncovalent, and mixed interactions. A promising way forward in the development of surface chemistry functionals, therefore, is to optimize the MS2 functional with a dispersion term. Screened hybrid functionals such as HSE06 are not only expensive but also yield accuracies similar to simple GGAs, thereby making them less attractive functionals for transition metal surface chemistry studies due to insufficient screening of exchange interactions for magnetic transition metals in particular.

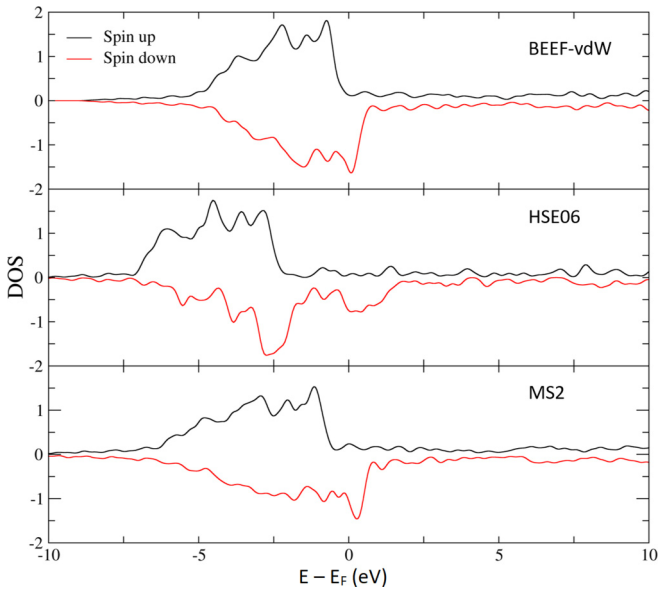

FIG. 7. Ni total DOS calculated with the following representative exchange-correlation (XC) functionals: BEEF-vdW, MS2, and HSE06.

The comparison between lattice constants and adsorption energies in the ADS41 dataset calculated using VASP and GPAW indicates a code specificity of Bayesian error estimation functionals. We thus recommend that Bayesian error estimation functionals be reparametrized in each code. If this is not possible, the pseudopotentials used in a certain code should be as similar as possible to those used to perform the original BEEF parametrization.

ACKNOWLEDGMENTS

This work is supported by the U.S. Department of Energy, Office of Science, Office of Basic Energy Sciences

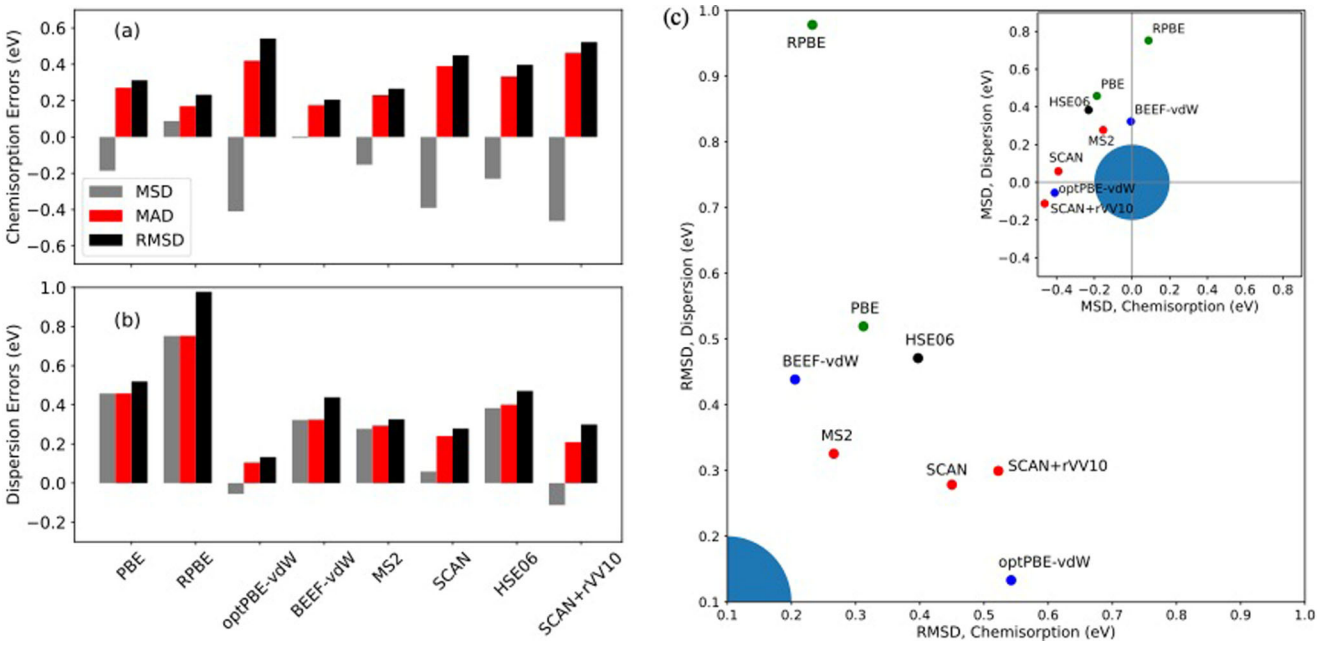

FIG. 8. Error statistics for (a) chemisorption and (b) dispersion energies calculated using PBE, RPBE, optPBE-vdW, BEEF-vdW, MS2, SCAN, and HSE06 functionals with the VASP code. (c) Bivariate plot of RMSD of the dispersion and chemisorption energies. Color code: green, GGAs; blue, dispersion-corrected GGAs; red, metaGGAs and dispersion-corrected metaGGA; black, hybrid functional. The shaded blue regions represent the ideal RMSD and MSD less than 0.2 eV.

provided through the SUNCAT Center for Interface Science and Catalysis. We are grateful to Prof. D. Truhlar's group at the University Minnesota for inputs on GGA adsorption energies.

APPENDIX A: MODEL SETUP

The model setups in this study are identical to those employed by Wellendorff *et al.* [9] for the systems constituting the CE39 dataset. The additional chemisorption system, ethene dissociation on Pt(111), is modeled using a four-layer 3×3 Pt(111) slab with the bottom two layers frozen. Naphthalene adsorption on Pt(111) is modeled using a four-layer 4×4 Pt(111) slab with the bottom two layers frozen.

APPENDIX B: CALCULATION PROCEDURE

A plane-wave cutoff energy of 700 eV was used for all the calculations in VASP and GPAW. Brillouin zone sampling is performed with a maximum k-point spacing of 0.02 Å^{-1}. A residual force threshold of 0.02 eV/Å for structural relaxations is employed. Four-layer slabs with the bottom two layers fixed and 15-Å vacuum between the surface species and the bottom of the repeated image of the slab are chosen for the slab calculations because four-layer slabs were used to yield accurate adsorption energies. A dipole correction was applied along the surface normal. Calculations of gas phase molecules were performed with supercells and at least 15 Å of vacuum spacing. Zero-point energy corrections for comparison to experiment are based in all considered cases on the PBE functional. Given that vibrational frequencies typically vary by less than 10% across different functionals [61] and the zero-point energy corrections are at most 15.6 kJ/mol in our calculations, the corresponding error will be at most 15 meV and hence negligible in this study. The convergence criteria are relaxed for the HSE06 functional owing to the high computational cost of tHe Hartree-Fock exchange: only the top layer of the slab is allowed to relax in all models. The cutoff energy is set to 400 eV, and the maximum spacing between k points is 0.03 Å^{-1} for Brillouin zone sampling. The force criterion is furthermore relaxed to 0.05 eV/Å.

[1] W. Kohn and L. J. Sham, Phys. Rev. **140**, A1133 (1965).
[2] W. Kohn, A. D. Becke, and R. G. Parr, J. Phys. Chem. **100**, 12974 (1996).
[3] B. G. Janesko, Top. Curr. Chem. **365**, 25 (2015).
[4] T. Bligaard, R. M. Bullock, C. T. Campbell, J. G. Chen, B. C. Gates, R. J. Gorte, C. W. Jones, W. D. Jones, J. R. Kitchin, and S. L. Scott, ACS Catal. **6**, 2590 (2016).
[5] P. Janthon, S. M. Kozlov, F. Viñes, J. Limtrakul, and F. Illas, J. Chem. Theory Comput. **9**, 1631 (2013).
[6] P. Janthon, S. A. Luo, S. M. Kozlov, F. Viñes, J. Limtrakul, D. G. Truhlar, and F. Illas, J. Chem. Theory Comput. **10**, 3832 (2014).
[7] L. Vega, J. Ruvireta, F. Viñes, and F. Illas, J. Chem. Theory Comput. **14**, 395 (2018).

[8] K. Raghavachari, G. W. Trucks, J. A. Pople, and M. Head-Gordon, Chem. Phys. Lett. **157**, 479 (1989).

[9] J. Wellendorff, T. L. Silbaugh, D. Garcia-Pintos, J. K. Nørskov, T. Bligaard, F. Studt, and C. T. Campbell, Surf. Sci. **640**, 36 (2015).

[10] K. Duanmu and D. G. Truhlar, J. Chem. Theory Comput. **13**, 835 (2017).

[11] A. J. R. Hensley, K. Ghale, C. Rieg, T. Dang, E. S. Anderst, F. Studt, C. T. Campbell, J.-S. McEwen, and Y. Xu, J. Phys. Chem. C **121**, 4937 (2017).

[12] T. L. Silbaugh and C. T. Campbell, J. Phys. Chem. C. **120**, 25161 (2016).

[13] K. Lejaeghere, G. Bihlmayer, T. Bjorkman, P. Blaha, S. Blugel, V. Blum, D. Caliste, I. E. Castelli, S. J. Clark, A. Dal Corso, S. de Gironcoli, T. Deutsch, J. K. Dewhurst, I. Di Marco, C. Draxl, M. Dułak, O. Eriksson, J. A. Flores-Livas, K. F. Garrity, L. Genovese, P. Giannozzi, M. Giantomassi, S. Goedecker, X. Gonze, O. Grånäs, E. K. U. Gross, A. Gulans, F. Gygi, D. R. Hamann, P. J. Hasnip, N. A. W. Holzwarth, D. Iuşan, D. B. Jochym, F. Jollet, D. Jones, G. Kresse, K. Koepernik, E. Kucukbenli, Y. O. Kvashnin, I. L. M. Locht, S. Lubeck, M. Marsman, N. Marzari, U. Nitzsche, L. Nordstrom, T. Ozaki, L. Paulatto, C. J. Pickard, W. Poelmans, M. I. J. Probert, K. Refson, M. Richter, G.-M. Rignanese, S. Saha, M. Scheffler, M. Schlipf, K. Schwarz, S. Sharma, F. Tavazza, P. Thunstrom, A. Tkatchenko, M. Torrent, D. Vanderbilt, M. J. van Setten, V. Van Speybroeck, J. M. Wills, J. R. Yates, G.-X. Zhang, and S. Cottenier, Science **351**, aad3000 (2016).

[14] S. Gautier, S. Steinmann, C. Michel, P. Fleurat-Lessard, and P. Sautet, Phys. Chem. Chem. Phys. **17**, 28921 (2015).

[15] W. A. Brown, R. Kose, and D. A. King, Chem. Rev. **98**, 797 (1998).

[16] J. M. Gottfried, E. K. Vestergaard, P. Bera, and C. T. Campbell, J. Phys. Chem. B. **110**, 17539 (2006).

[17] S. Mallikarjun Sharada, T. Bligaard, A. C. Luntz, G.-J. Kroes, and J. K. Nørskov, J. Phys. Chem. C **121**, 19807 (2017).

[18] C. T. Campbell and J. R. V. Sellers, Chem. Rev. **113**, 4106 (2013).

[19] C. T. Campbell and O. Lytken, Surf. Sci. **603**, 1365 (2009).

[20] J. P. Perdew, K. Burke, and M. Ernzerhof, Phys. Rev. Lett. **77**, 3865 (1996).

[21] J. P. Perdew and K. Schmidt, AIP Conf. Proc. **577**, 1 (2001).

[22] B. Hammer, L. B. Hansen, and J. K. Nørskov, Phys. Rev. B **59**, 7413 (1999).

[23] J. Wellendorff, K. T. Lundgaard, A. Møgelhøj, V. Petzold, D. D. Landis, J. K. Nørskov, T. Bligaard, and K. W. Jacobsen, Phys. Rev. B. **85**, 235149 (2012).

[24] J. Sun, R. Haunschild, B. Xiao, I. W. Bulik, G. E. Scuseria, and J. P. Perdew, J. Chem. Phys. **138**, 044113 (2013).

[25] J. Sun, B. Xiao, Y. Fang, R. Haunschild, P. Hao, A. Ruzsinszky, G. I. Csonka, G. E. Scuseria, and J. P. Perdew, Phys. Rev. Lett. **111**, 106401 (2013).

[26] J. Sun, A. Ruzsinszky, and J. P. Perdew, Phys. Rev. Lett. **115**, 036402 (2015).

[27] H. Peng, Z.-H. Yang, J. P. Perdew, and J. Sun, Phys. Rev. X **6**, 041005 (2016).

[28] P. Giannozzi, S. Baroni, N. Bonini, M. Calandra, R. Car, C. Cavazzoni, D. Ceresoli, G. L. Chiarotti, M. Cococcioni, I. Dabo, A. D. Corso, S. de Gironcoli, S. Fabris, G. Fratesi, R. Gebauer, U. Gerstmann, C. Gougoussis, A. Kokalj, M. Lazzeri, L. Martin-Samos, N. Marzari, F. Mauri, R. Mazzarello, S. Paolini, A. Pasquarello, L. Paulatto, C. Sbraccia, S. Scandolo, G. Sclauzero, A. P. Seitsonen, A. Smogunov, P. Umari, and R. M. Wentzcovitch, J. Phys. Condens. Matter **21**, 395502 (2009).

[29] A. A. Adllan and A. D. Corso, J. Phys Condens. Matter **23**, 425501 (2011).

[30] G. Kresse and J. Hafner, Phys. Rev. B **47**, 558 (1993).

[31] G. Kresse and J. Hafner, Phys. Rev. B **49**, 14251 (1994).

[32] G. Kresse and J. Furthmüller, Phys. Rev. B **54**, 11169 (1996).

[33] P. E. Blöchl, Phys. Rev. B **50**, 17953 (1994).

[34] G. Kresse and D. Joubert, Phys. Rev. B **59**, 1758 (1999).

[35] J. J. Mortensen, L. B. Hansen, and K. W. Jacobsen, Phys. Rev. B. **71**, 035109 (2005).

[36] J. Enkovaara, C. Rostgaard, J. J. Mortensen, J. Chen, M. Dułak, L. Ferrighi, J. Gavnholt, C. Glinsvad, V. Haikola, H. A. Hansen, H. H. Kristoffersen, M. Kuisma, A. H. Larsen, L. Lehtovaara, M. Ljungberg, O. Lopez-Acevedo, P. G. Moses, J. Ojanen, T. Olsen, V. Petzold, N. A. Romero, J. Stausholm-Møller, M. Strange, G. A. Tritsaris, M. Vanin, M. Walter, B. Hammer, H. Häkkinen, G. K. H. Madsen, R. M. Nieminen, J. K. Nørskov, M. Puska, T. T. Rantala, J. Schiøtz, K. S. Thygesen, and K. W. Jacobsen, J. Phys.: Condens. Matter **22**, 253202 (2010).

[37] P. Haas, F. Tran, and P. Blaha, Phys. Rev. B **79**, 085104 (2009).

[38] F. Tran, J. Stelzl, and P. Blaha, J. Chem. Phys. **144**, 204120 (2016).

[39] J. Klimeš, D. R. Bowler, and A. Michaelides, J. Phys: Condens. Matter **22**, 022201 (2010).

[40] R. Sabatini, T. Gorni, and S. de Gironcoli, Phys. Rev. B **87**, 041108(R) (2013).

[41] A. V. Krukau, O. A. Vydrov, A. F. Izmaylov, and G. E. Scuseria, J. Chem. Phys. **125**, 224106 (2006).

[42] K. T. Winther, M. J. Hoffmann, J. R. Boes, O. Mamun, M. Bajdich, and T. Bligaard, Sci. Data **6**, 75 (2019).

[43] M. Dion, H. Rydberg, E. Schröder, D. C. Langreth, and B. I. Lundqvist, Phys. Rev. Lett. **92**, 246401 (2004).

[44] J. J. Mortensen, K. Kaasbjerg, S. L. Frederiksen, J. K. Nørskov, J. P. Sethna, and K. W. Jacobsen, Phys. Rev. Lett. **95**, 216401 (2005).

[45] K. Lee, É. D. Murray, L. Kong, B. I. Lundqvist, and D. C. Langreth, Phys. Rev. B **82**, 081101(R) (2010).

[46] J. Hermann, R. A. DiStasio, and A. Tkatchenko, Chem. Rev. **117**, 4714 (2017).

[47] A. J. Garza, A. T. Bell, and M. Head-Gordon, J. Chem. Theory Comput. **14**, 3083 (2018).

[48] J. Witte, N. Mardirossian, J. B. Neaton, and M. Head-Gordon, J. Chem. Theory Comput. **13**, 2043 (2017).

[49] L. A. Constantin, E. Fabiano, J. M. Pitarke, and F. Della Sala, Phys. Rev. B **93**, 115127 (2016).

[50] L. A. Constantin, E. Fabiano, and F. Della Sala, Phys. Rev. B **88**, 125112 (2013).

[51] J. Tao and Y. Mo, Phys. Rev. Lett. **117**, 073001 (2016).

[52] J. Wellendorff, K. T. Lundgaard, K. W. Jacobsen, and T. Bligaard, J. Chem. Phys. **140**, 144107 (2014).

[53] K. T. Lundgaard, J. Wellendorff, J. Voss, K. W. Jacobsen, and T. Bligaard, Phys. Rev. B. **93**, 235162 (2016).

[54] Y. Zhao and D. G. Truhlar, J. Chem. Phys. **125**, 194101 (2006).
[55] A. Patra, H. Peng, J. Sun, and J. P. Perdew, arXiv:1807.05450.
[56] P. J. Feibelman, B. Hammer, J. K. Nørskov, F. Wagner, M. Scheffler, R. Stumpf, R. Watwe, and J. Dumesic, J. Phys. Chem. B **105**, 4018 (2001).
[57] A. Stroppa, K. Termentzidis, J. Paier, G. Kresse, and J. Hafner, Phys. Rev. B **76**, 195440 (2007).
[58] G. Kresse, A. Gil, and P. Sautet, Phys. Rev. B **68**, 073401 (2003).
[59] A. Stroppa and G. Kresse, New J. Phys. **10**, 063020 (2008).
[60] A. Notario-Estévez, S. M. Kozlov, F. Viñes, and F. Illas, Chem. Commun. **51**, 5602 (2015).
[61] A. P. Scott and L. Radom, J. Phys. Chem. **100**, 16502 (1996).